THESIS FOR THE DEGREE OF LICENTIATE OF ENGINEERING

Spectroscopic characterisation of surface hydroxyls during catalytic methane oxidation

PETER VELIN

CHALMERS

Department of Chemistry and Chemical Engineering
CHALMERS UNIVERSITY OF TECHNOLOGY
Gothenburg, Sweden 2018

Spectroscopic characterisation of surface hydroxyls during catalytic methane oxidation
PETER VELIN

Licentiatuppsatser vid Institutionen för kemi och kemiteknik
Chalmers tekniska högskola
Nr 2018:05

Department of Chemistry and Chemical Engineering
Chalmers University of Technology
SE-412 96 Gothenburg
Telephone +46 31 772 2938

Typeset in LaTeX
Printed by Chalmers Reproservice
Gothenburg, Sweden 2018

Spectroscopic characterisation of surface hydroxyls during catalytic methane oxidation

PETER VELIN
Department of Chemistry and Chemical Engineering
Chalmers University of Technology

Abstract

Implementation of methane rich fuels as to develop sustainable vehicle transports requires improved catalytic exhaust aftertreatment technologies to convert engine-out methane emissions to carbon dioxide and water by total oxidation. A main challenge is that water formed during combustion inhibits the methane oxidation reaction even over the most active palladium-based catalysts presently known. This work aims at elucidating the active state of palladium and main deactivating mechanism(s) caused by water for alumina supported palladium catalysts to build fundamental knowledge about how catalysts with improved water tolerance can be designed.

A bottom-up research approach including synthesis, characterisation and evaluation of single catalyst components and model catalysts has been employed. In specific, *operando* X-ray absorption spectroscopy and diffuse reflectance infrared Fourier transform spectroscopy have been used to monitor the oxidation state of palladium and adsorbed hydroxyls. A portable water generator device was constructed to ensure accurate feed concentrations of pure water vapor for spectroscopic characterisation.

For Pd/γ-Al_2O_3, oxygen pulse-response methane oxidation experiments reveal high catalytic activity for both reduced Pd and well-developed PdO. The transition between these two states depends on oxygen concentration and temperature and is associated with lower catalytic activity. During dry methane oxidation, terminal and bridge-bonded hydroxyl species evolve and upon water addition the hydroxyl coverage increases further, which correlates well with a decreased catalytic activity both for short (1 h) and long (24 h) periods. The availability of alumina Lewis acid sites dictates the formation of hydroxyl species such that when modified with Pd, fewer hydroxyl groups are detected for catalysts with high Pd dispersion. Surface hydroxyl formation routes and kinetics role of boundary sites for high catalytic activity are discussed.

Keywords: Sustainable transports; Environmental catalysis; Methane oxidation; Supported palladium; Water inhibition; *Operando* spectroscopy; DRIFTS; XAS

List of Publications

This thesis is based on the work contained in the following appended publications:

I. Oxygen step-response experiments for methane oxidation over Pd/Al_2O_3: An in situ XAFS study

J. Nilsson, P.-A. Carlsson, N. M. Martin, P. Velin, D. Motta-Meira, H. Grönbeck and M. Skoglundh

Catal. Comm., DOI:10.1016/j.catcom.2018.02.011.

II. Portable device for generation of ultra-pure water vapor feeds

P. Velin, U.Stenman, M. Skoglundh and P.-A. Carlsson

Rev. Sci. Instrum., **88** (2017), 115102-115109

III. Vibrational study on water inhibition of lean methane oxidation over Pd/Al_2O_3 model catalysts

P. Velin, M. Skoglundh, G. Smedler, A. Raj, D. Thompsett, and P.-A. Carlsson

Submitted to ACS Catalysis

Additional publications, not included in this thesis:

Characterization of Surface Structure and Oxidation/Reduction Behavior of Pd-Pt/Al_2O_3 Model Catalysts

N. M. Martin, J. Nilsson, M. Skoglundh, E. C. Adams, X. Wang, P. Velin, G. Smedler, A. Raj, D. Thompsett, H. H. Brongersma, T. Grehl, G. Agostini, O. Mathon, S. Carlson, K. Norén, F. J. Martinez-Casado, Z. Matej, O. Balmes and P.-A. Carlsson

J. Phys. Chem. C, **120** (2016), 28009-28020

Catalytic hydrogenation of CO_2 to methane over supported Pd, Rh and Ni catalysts

N. M. Martin, P. Velin, M. Skoglundh, M. Bauer and P.-A. Carlsson

Catal. Sci. Technol., **7** (2017), 1086-1094

CO oxidation and Site Speciation for Alloyed Palladium-Platinum Model Catalysts Studied by *in Situ* FTIR spectroscopy

N. M. Martin, M. Skoglundh, G. Smedler, A. Raj, D. Thompsett, P. Velin, F. J. Martinez-Casado, Z. Matej, O. Balmes and P.-A. Carlsson

J. Phys. Chem. C, **121** (2017), 26321-26329

My contribution to the papers

Paper I

I participated in catalyst preparation, XAS measurements at the European Synchrotron Radiation Facility (ESRF), and co-authored the manuscript.

Paper II

I participated in the design and construction of the portable water generation device, performed the experimental work and data analysis, interpreted the results with my co-authors and was responsible for writing the first draft and submission of the manuscript.

Paper III

I performed the experimental work, data analysis, interpreted the results with my co-authors and was responsible for writing the first draft and submission of the manuscript.

CONTENTS

1 Introduction **1**

1.1 Methane emission abatement 2

1.2 Objectives 3

2 Background **5**

2.1 Methane oxidation catalysts 5

2.2 Catalyst deactivation 6

2.2.1 Mechanisms 6

2.2.2 Water inhibition 8

3 Research approach, materials and methods **11**

3.1 Bottom-up methodology 11

3.2 Sample preparation 12

3.3 Physicochemical characterisation 13

3.3.1 Nitrogen physisorption 13

3.3.2 Carbon monoxide chemisorption 13

3.3.3 X-ray powder diffraction 14

3.4 *Operando* spectroscopy 15

3.4.1 X-ray absorption spectroscopy 15

3.4.2 Infrared probing 16

3.4.3 Fourier transform infrared spectroscopy 17

3.4.4 Diffuse reflectance infrared Fourier transform spectroscopy 17

4 Results and Discussion **19**
4.1 Active state of Pd during lean methane oxidation 19
4.2 Methane oxidation in dry and wet conditions 21
4.2.1 Accurate and precise water delivery 21
4.2.2 Surface hydroxyls on single catalyst components 22
4.2.3 Surface hydroxyls on alumina supported Pd model catalysts . . . 24

5 Concluding remarks **29**

Acknowledgements **31**

Bibliography **33**

CHAPTER 1

INTRODUCTION

The shift from coal to natural gas in the heat and power generation sectors led in 2015, for the first time since 1990s, to a reduction in global greenhouse gas (GHG) emissions whilst the global economy grew [1]. This is because the principal component in natural gas is methane (CH_4), which possesses the highest hydrogen-to-carbon ratio of all hydrocarbons in fossil fuels. Longer hydrocarbons such as ethane and propane are minor constituents [2]. Hence, natural gas combustion generates the lowest amount of carbon dioxide (CO_2) per unit of energy released [3]. The shift to natural gas combustion also benefits the local environment due to reduced emissions of nitrogen oxides (NO_x), sulphur oxides (SO_x) and particulate matter [4]. Although these emission reductions are good incentives for increased use of natural gas as to shift the energy system to become more sustainable, abundant and readily available reserves worldwide should be considered as the primary reason for the increased market shares of natural gas [5].

The transport sector accounts for about a quarter of the global GHG emissions [1]. In response, as to meet the ever stricter emission standards, companies developing vehicle powertrains are considering using natural gas as fuel thanks to the advantages mentioned above. Without judging on technology choices, the Volkswagen emission scandal, known as dieselgate, recently led to societal discussions about severe pollution from diesel vehicles. The public's concern of global warming and poor air quality, particularly in urban areas (cities), may also drive the pursuit of upcoming technologies. Biogas is a renewable fuel that to large extent resembles natural gas with its clean burning properties. Natural gas and biogas mixtures in any proportions are possible, making

the CH_4 rich fuels a plausible candidate in a more sustainable future fuel mixture less dependent on conventional fossil fuels. It should be mentioned, however, that CH_4 is a potent GHG with a global warming potential 28 times higher than CO_2 over a 100-year period [6]. Emissions of methane from vehicles must therefore be avoided.

1.1 Methane emission abatement

Catalytic converters can be incorporated in the exhaust system as an end-of-pipe solution to prevent that CH_4 slipped through the engine is reaching the atmosphere. By use of appropriate catalyst formulations and operation strategies, emissions of various detrimental compounds can be controlled. In the case of engine-out methane emissions, these should be oxidised (combusted) to carbon dioxide and water. The catalyst used in automotive aftertreatment systems relies on heterogeneous catalysis, where a solid material, the catalyst, increases the overall chemical reaction rate of gaseous reactants by enabling an alternative, energetically favourable, reaction path. Unlike simple gas phase reactions with a large single energy barrier, catalytic reactions take place in several steps [7]. The initial step is adsorption of the reactants on the surface. Conversion of the adsorbed reactants to products is then mediated by formation of new bonds in a surface reaction. Finally, adsorbed products are desorbed into the gas phase in the last step. In order to achieve an overall high efficiency of the catalytic cycle, surface-adsorbate bonds should neither be too weak nor too strong, recognized as the Sabatier principle [8]. Furthermore, the active sites will continuously be regenerated at the end of the catalytic cycle and the catalyst will hence not be consumed.

Methane is the most difficult hydrocarbon to oxidise catalytically due to its symmetrical tetrahedral shape with non-polar C-H bonds and low sticking probability, which leads to poor adsorption [9, 10]. This is reflected by the relatively high temperatures required to oxidise methane even over the most efficient catalytic converters presently known. Mitigation of CH_4 is thus problematic and will be even more so in future vehicles as the development of more efficient engines inevitably leads to lower engine-out temperatures. Furthermore, high water vapor concentration in the exhaust gas is another issue that has been found to reduce the catalytic methane oxidation activity at temperatures as high as 600 °C [11–14]. The trial-and-error approaches used for decades have not led to considerable improvements of catalyst formulations with respect to water tol-

erance. In this work, a bottom-up methodology has been employed to investigate the inhibiting effect of water vapor on methane oxidation over traditionally used aluminum oxide supported palladium catalysts (Pd/Al_2O_3). A portable water vapor generator device has been constructed that enables reliable and reproducible spectroscopic measurements of water inhibited methane oxidation both at Chalmers and other international research facilities.

1.2 Objectives

The objective of this thesis is to investigate water inhibition mechanisms of lean methane oxidation in dry and wet conditions observed for Pd/Al_2O_3 catalysts. Employing *operando* spectroscopic techniques and a bottom-up research approach, the active states of Pd and formation/decomposition of hydroxyl species were investigated at different temperatures in the absence and presence of water during methane oxidation.

CHAPTER 2
BACKGROUND

2.1 Methane oxidation catalysts

Catalysts used for total oxidation of hydrocarbons are typically composed of a noble metal active phase, highly dispersed over a porous metal oxide, which is called the support (left part of Figure 2.1). To make use of the expensive active material one strive for catalysts with high dispersion, which results in a myriad of noble metal nanoparticles on the support surface. Low amounts of promoting elements are often added to increase the catalytic activity of fully formulated catalysts. To ensure high reactant-catalyst interaction and low pressure drop of the exhaust feed in mobile aftertreatment systems, the catalyst is commonly washcoated onto a honeycomb structured monolith substrate [15].

Palladium has for decades been considered as the most active element for total oxidation of methane [16–18]. This work will thus focus on palladium model catalysts, where the active phase is distributed over porous aluminum oxides (Al_2O_3). Al_2O_3 in various forms (γ, η, θ and δ) is commonly used as support materials in heterogeneous catalysis due to its large surface area, refractory properties, good interaction with the active phase and cost efficiency [19]. Although, the support material already highly stabilises the catalyst, the addition of platinum to form bimetallic Pd-Pt alloys, shows promising results in terms of further increased stability over time [20–24].

The major challenges and great interest in improving methane oxidation catalysts have resulted in a plethora of publications in the field. New types of catalyst formu-

lations such as bimetallic alloys supported by metal oxides, perovskites, spinels and core-shell structures are examples of up-and-coming emerging technologies [25–31]. However, for these formulations to enter industrial realization, large-scale production with a commercially viable price is required.

2.2 Catalyst deactivation

It is important to reflect on the fact that the catalyst formulation with highest activity in laboratory environments is not necessarily the most appropriate one in practice. The reality is more complex and dynamic than laboratory tests with, e.g., optimal reactant mixtures at steady state temperatures. This means that numerous of performance measurements in various conditions are required.

To ensure that an operating catalytic converter fulfill the emission limits over time, new emission standards include follow-up tests after a certain number of years or driven distance. Causes behind catalyst deterioration is important for manufactures to consider when durable formulations less susceptible to deactivation are designed. In the coming section, the most common deactivation mechanisms in automotive aftertreatment applications are described. Finally, the inhibiting effect of water vapor on methane oxidation catalysts reported in literature is discussed.

2.2.1 Mechanisms

Although a catalyst is not consumed in stoichiometric amounts in a catalytic reaction, the high initial activity observed for a fresh catalyst may decrease during operation. Catalyst deactivation is usually due to loss of active sites. Figure 2.1 illustrates four different mechanisms where active sites may be lost, known as: (a) thermal degradation, (b) poisoning, (c) fouling and (d) vapor compound formation [32].

As shown in Figure 2.1a, thermal deactivation leads to decreased active phase area via aggregation of the dispersed metal nanoparticles to larger ones. The phenomenon, often referred to as sintering is facilitated by high reaction temperatures ($>500^{\circ}$C) and is generally increased in the presence of water vapor (hydrothermal degradation) [32]. Two additional issues with high temperature operation, not included in the Figure 2.1, are support sintering and active phase transformation. Support sintering gives rise to partial or total blockage of some pores, which complicates internal reactant diffusion

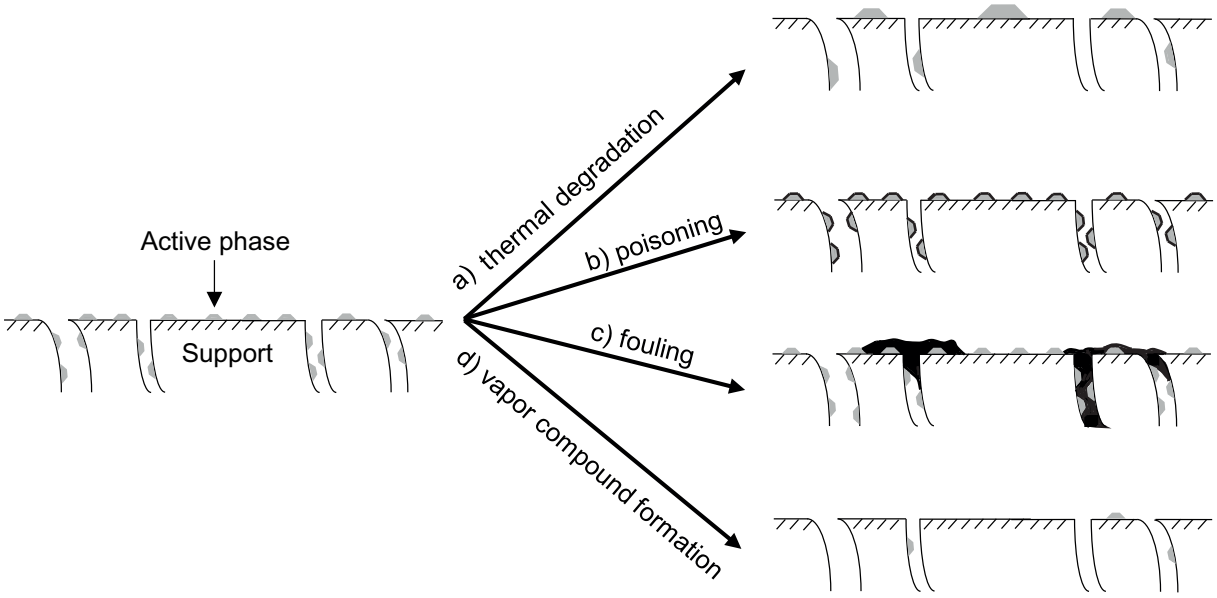

Figure 2.1: Conceptual model of thermal degradation, poisoning, fouling and vapor compound formation as deactivation mechanisms for a model catalyst.

and decreases the availability of active sites. Active phase transformation is a type of thermal degradation where the active phase is transformed to a less- or non-catalytically active phase.

Another deactivation mechanism, illustrated as black lines enclosing the active phase in Figure 2.1b, is poisoning. This is a chemical deactivation where a compound interacts with the catalyst and decreases the activity. Depending on its adsorption strength to the concerned sites relative to competing species, a compound or element is considered as a strong, intermediate or weak poison. Increased toxicity is seen for larger poison species with high electronegativity that physically blocks active sites through strong adsorption [32]. Elements like sulphur and phosphorus as well as molecules like carbon monoxide and nitrogen oxide are recognized as poisons that deteriorate the catalyst performance by physical blockage. Strong adsorbate-surface bonds may furthermore have negative effects on; (i) neighbouring sites electronically, (ii) surface structure and (iii) reactant surface diffusion [32].

A third mechanism associated with heterogeneous catalyst deactivation is fouling (Figure 2.1c). Fouling occurs due to deposition of a physical compound, typically carbon based [32], that blocks active sites on the catalyst surface. Increased coverages of deposited compounds can lead to more extensive blockage, e.g. of pores in the support. This will hinder reactants from reaching the large number of the active sites located in

the pores, with drastically reduced activity as a consequence.

Volatile compound formation is the final type of deactivating phenomenon mentioned in this thesis. As the name indicates, it involves loss of catalytic material by formation of volatile compounds. Gaseous environment, catalyst components and reaction temperature are three major aspects that needs to be consider in order to prevent the catalyst from being consumed. A classical example is the detrimental combination of carbon monoxide exposure to nickel catalysts, which may result in formation of poisonous volatile carbonyl compounds, $Ni(CO)_4$ [32]. Another risky example is formation of volatile metal oxides of ruthenium, lead or platinum based catalysts exposed to oxygen at high temperatures [32].

2.2.2 Water inhibition

The high water vapor concentrations ($\sim$12 vol.%) in the engine exhaust is severely problematic to traditional supported palladium methane oxidation catalysts due to their high susceptibility to become inhibited by water. No general agreement on how to explain the observed kinetic effects has yet been reached and more fundamental studies are therefore required. Kinetic flow reactor measurements have shown a rapidly decreased catalytic activity when water is added to a dry feed of methane and oxygen [33, 34]. It has also been shown that the effect is almost completely reversible and initial activity will generally be regenerated by high temperature treatment [28, 35]. As already mentioned, high temperature exposure in wet conditions should be performed with caution due to the risk of hydrothermal degradation.

In several early studies, the mechanism for inhibited meyhane oxidation was explained by the formation of a palladium hydroxide ($Pd(OH)_2$) phase, much less active than PdO [36–39]. More recently proposed mechanisms attribute the water inhibition to increased coverage of hydroxyl (OH) groups on the catalyst surface, and the reversibility is then due to increased water desorption rate at elevated temperature [40, 41]. Specific knowledge about the concerned sites and whether additional mechanisms than solely physical blockage occurs is however lacking. It has been suggested that an increased coverage of hydroxyl groups on the support surface may reduce oxygen transport to the active palladium phase [41, 42]. The main part of oxygen in the final products is considered to originate from bulk PdO following a redox Mars-van Krevalen mechanism [42–45]. Gas phase oxygen is required to reoxidise the active

sites in the lattice and a decreased oxygen access means slower regeneration, leading to lower catalytic activity.

In addition to the instantaneous response of altered water vapor concentrations in the feed, a slower, less reversible deactivation has been observed in long time exposure experiments [21, 35]. Decreased palladium oxide dispersion as an effect of particle growth has been suggested the main cause of this catalyst deactivation [46, 47].

CHAPTER 3

RESEARCH APPROACH, MATERIALS AND METHODS

3.1 Bottom-up methodology

The development of catalysts has mainly followed a trial-and-error approach, which often is fast, but the implementation of new formulations for methane oxidation has been slow compared to other emission control technologies. Hence in this work a bottom-up research approach, illustrated in Figure 2.1, is used to increase the fundamental understanding of the inhibiting effect of water vapor on methane oxidation over Pd/Al_2O_3. Gas-fueled vehicles commonly operates in fuel lean conditions, i.e. in oxygen excess, where palladium is in an oxidised state at operating temperatures [48–50]. Detailed X-ray absorption spectroscopic measurements reported by our research group has shown that this holds for both the platinum and palladium phases in supported catalysts [24, 51–53], and is demonstrated for a Pd/Al_2O_3 model catalyst in paper I.

To eliminate complications of interactions between different catalyst constituents, the single components (PdO and Al_2O_3) of a Pd/Al_2O_3 model catalyst were investigated. Assignment of surface-bound species (mainly hydroxyls) on respective component was enabled by exposure to oxygen, methane, water and argon gas mixtures. The temperature influence on hydroxyl stability on the surface was probed by infrared spectroscopy. Single component insight about surface-bound species was compared to model catalysts of low complexity to understand improved reaction kinetics for the combined PdO-Al_2O_3 systems. Model catalysts with both high and low palladium dispersion were prepared to relate a smaller particle size to increased catalytic activity. This means various PdO

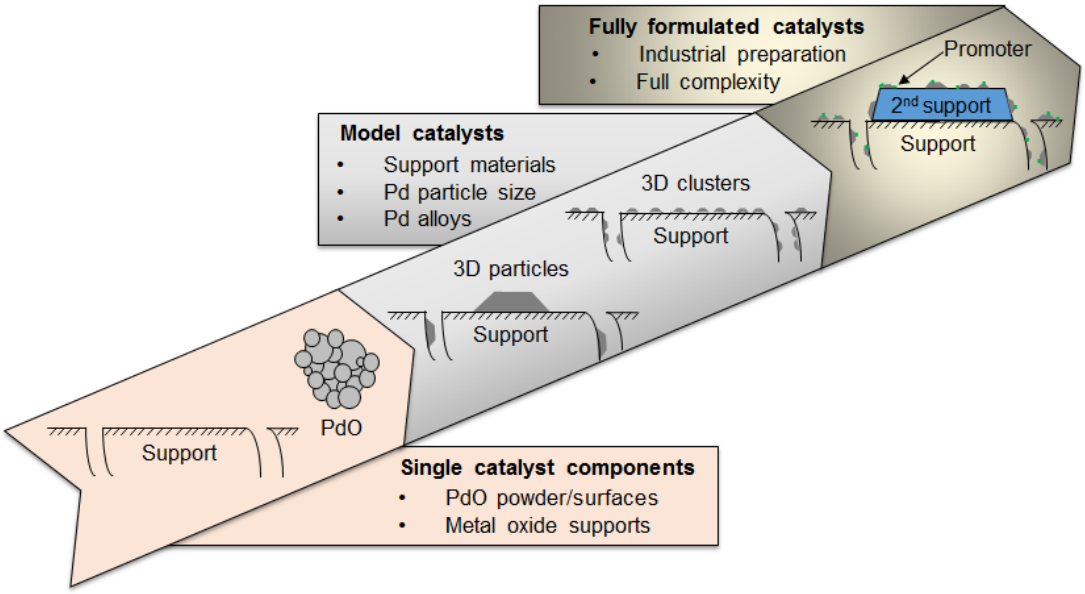

Figure 3.1: Bottom-up approach, used to study single catalyst components, model catalysts of varying complexities and fully formulated catalysts.

coverages on the alumina surface, which further increase the understanding of coveted support properties. For model catalysts with a majority of PdO clusters, i.e. small particles consisting of a few atoms, a promoting effect of the Al_2O_3 support itself may give rise to an increased catalytic activity.

Working with simplified systems is a way to bridge the materials gap in knowledge between single crystals and industrial catalysts. The findings received from bottom-up investigation will be useful in a later step when fully formulated catalysts with high complexity will be developed towards specific properties, such as high water tolerance.

3.2 Sample preparation

The incipient wetness impregnation (IWI) technique was used to prepare the supported palladium model catalysts investigated in this work. IWI is frequently used in industrial catalyst production due to its simple execution and low waste streams [54]. Preparation started with thermal treatment of the support material (γ-Al_2O_3) in air to remove impurities and stabilise the structure. An even distribution and dispersion of the active phase over the support was ensured by adding the required volume of palladium precursor solution and water to fill the Al_2O_3 pores, utilizing the natural capillary pressure difference [54]. The slurry was pH adjusted to receive high electrostatic interaction be-

tween metal precursor and support. Solvent and complex agents were finally removed by thermal treatment of the samples in air at temperatures ranging from 500 to 900°C.

3.3 Physicochemical characterisation

3.3.1 Nitrogen physisorption

To determine the specific surface area (SA_{total}) of mesoporous samples, nitrogen physisorption measurements were used in paper II and III. The analysis is performed by controlled increments of nitrogen that adsorbs onto the sample surface. In addition to the sorption measurements, a theoretical method such as BET theory is required for SA determination [55, 55]. BET theory is an extension of the Langmuir theory for monolayer adsorption, where it is assumed that the adsorbate's partial pressure is related to the volume adsorbed onto the adsorbent. Assumptions in BET calculations are; (i) nitrogen gas molecules behave ideally, (ii) only one monolayer is formed, (iii) all sites on the surface are equal, (iv) no adsorbate-adsorbate interaction, (v) adsorbates are immobile. Thanks to a linear relationship of the BET equation (3.1) at low partial pressures, the required volume of nitrogen to form a monolayer on the sample (V_m) can be obtained by interpolation.

$$\frac{P}{V(P_0 - P)} = \frac{C-1}{V_m\, C}\frac{P}{P_0} + \frac{1}{V_m\, C} \tag{3.1}$$

P and P_0 are equilibrium and saturation pressure of adsorbates at the temperature of adsorption, V is the volume of adsorbed gas and C is the BET constant. The specific surface area is then calculated according to equation 3.2, where s is the cross section of the adsorbate, V is the molar volume of the adsorbate gas, and m is the sample mass.

$$SA_{total} = \frac{6.022\ 10^{23}\ V_m\ s}{V\ m} \tag{3.2}$$

3.3.2 Carbon monoxide chemisorption

The noble-metal surface area, dispersion and particle size of a supported catalyst was measured by selective carbon monoxide (CO) chemisorption in paper III. The procedure relies on strong interaction between the chemisorbed CO adsorbate and the active metal atom(s), typically involving the sharing of electrons. The chemisorbed CO layer is

assumed to not exceed a single molecule thickness [56]. For generation of reliable and reproducible results, the samples in this work were prior to analysis oxidised, reduced and evacuated (<10 μmHg) at 350 °C for one hour each. The reduced noble-metal surface of the samples were then exposed to absolute pressure increments of 50 mmHg CO between 100-450 mmHg. At each increment, the pressure was allowed to reach equilibrium and the adsorbed quantity was measured. From this information the metallic surface area per gram of sample was calculated according to equation 3.3, where $V_{intercept}$ is the volume intercept derived from the best line fit of the isotherm (quantity adsorbed vs pressure), A is the effective area of 1 noble metal atom and 22414 is the volume one mole of gas occupies at standard temperature and pressure. CO was also assumed to chemisorb on palladium with a bridged configuration, giving a CO:Pd ratio of 1:2 and hence a stoichiometric factor (S_F) of 2 [56].

$$SA_{active} = \frac{6.022\ 10^{23}\ V_{intercept}\ A\ S_F}{22414} \tag{3.3}$$

3.3.3 X-ray powder diffraction

Powder X-ray diffraction (XRD) is a non-destructive technique to determine crystalline bulk structures within the catalyst. Measurements were performed by radiating the powder sample with monochromatic X-rays and varying the incident angle (θ). The X-ray wavelength (λ) is of the same order of magnitude as the spacing (d) between diffracting planes in the lattice. Constructive interference occurs at specific angles when elastically scattered X-ray beams from different planes are in phase. This is in accordance to the Bragg equation (3.4), where n is an integer [57]. The provided diffraction patterns with increased intensity at particular angles can be correlated to their specific crystal structures.

$$n\ \lambda = 2\ d\ sin\theta \tag{3.4}$$

An estimation of the apparent nobel-metal crystallite size ($d_{particle}$) was furthermore calculated in paper I, II and III using the Sherrer equation (3.5), where κ is a dimensionless shape factor, λ is the X-ray wavelength, β is the full width at half maximum and θ is the Bragg angle. However, the method is limited to grains smaller than 0.2 μm and does not consider particles with too short crystalline order (<3nm) [58].

$$d_{particle} = \frac{\kappa\ \lambda}{\beta\ cos\theta} \tag{3.5}$$

3.4 *Operando* spectroscopy

Operando spectroscopy, i.e., where a spectroscopic characterisation, usually as a time-resolved measurement, is carried out while the function of the system under study, here the catalytic reaction, is increasingly used in catalysis research [59, 60]. By combining the characterisation technique with online product analysis, one can relate fundamental information about the electronic and molecular structures of active sites and surface intermediates to changes in catalytic kinetics. This type of understanding is highly valuable when new catalyst formulations with improved properties are developed for specific applications. In this thesis X-ray absorption and infrared spectroscopy has been used to follow the chemical state and local structure of the palladium phase and the surface adsorbates, respectively. Simultaneously, mass spectrometry measurements has been carried out to follow the reactant conversion and product selectivity. The main topic of the thesis, however, is on the role of surface hydroxyls and thus the methodological description of infrared spectroscopy is somewhat more detailed than for the X-ray absorption spectroscopy measurements.

3.4.1 X-ray absorption spectroscopy

X-ray absorption spectroscopy (XAS) is a technique that utilise the ability of core-shell electrons to absorb X-rays of definite energies. Typically a synchrotron light source is required to provide enough brightness, i.e. a high flux of x-rays [61]. XAS data can be divided into low and high energy regions called X-ray Absorption Near-Edge Structure (XANES) and Extended X-ray Absorption Fine Structure (EXAFS), respectively. In paper I, the XANES region was analysed to obtain information about oxidation state of the palladium(oxide) phase. Practically, energy-dispersive measurements were performed at the Pd K edge with an energy range of 23 500 to 26 500 using a polychromator. The polychromator is an optical device that allows measurements of an entire absorption spectrum in less than a second by dispersing the light into different directions [62]. The dispersed light consists of a range of wavelength and high time-resolution is enabled

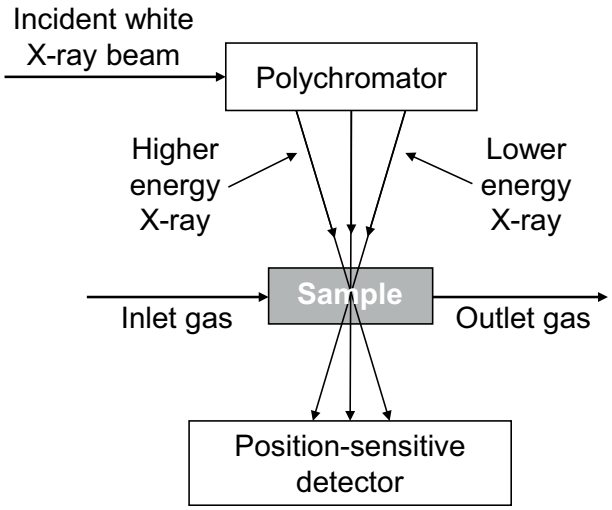

Figure 3.2: Schematic of energy-dispersive XAS setup

by focusing the X-rays on the sample and measure the transmitted light by a position-sensitive detector, see Figure 3.2.

3.4.2 Infrared probing

Infrared probing relies on the interaction between infrared photons and matter. Interaction occurs as energy absorption at resonant frequencies, i.e. when the frequency of a photon matches the vibrational mode of a chemical bond, giving rise to a change in dipole moment [63]. The frequency of an absorption band is referred to as the wavenumber (ν), and its energy is simply related to the strength of the bond and the atom mass at either end of it. The degrees of vibrational modes of a molecule differ depending on shape and number of atoms (N). A linear molecule have 3N – 5 bands while a non-linear have 3N – 6. This means that a non-linear triatomic molecule like water has 3 vibrational modes. These modes are illustrated in Figure 3.3 and corresponds to symmetric stretching (ν_1) at 3657 cm^{-1}, deformation (ν_2) at 1596 cm^{-1} and antisymmetric stretching (ν_3) at 3756 cm^{-1} [63]. The lack of dipole moment makes the symmetric stretching band IR inactive and only two of the vibrational bands (ν_2 and ν_3) can be detected by IR spectroscopy. However, due to a small moment of inertia on rotation, tens of thousands vibrational-rotational absorption bands can arise for water molecules in gas phase.

3.4.3 Fourier transform infrared spectroscopy

Fourier transform infrared (FTIR) spectroscopy is a commonly used technique to obtain an infrared spectrum that can be used to identify solid, liquid or gas phase molecules. The top left part of Figure 3.4 illustrates how the Michelson interferometer, causes interference of infrared light [63]. This is enabled by a beamsplitter that divides the radiation from the IR source in two partial beams that are reflected back to the beamsplitter on a fixed and on a movable mirror. Back at the beamsplitter each wavelength of the light is periodically blocked and transmitted due to the difference in optical pathlength produced by the movable mirror. Some of the recombined light is directed towards the IR source by the beamsplitter and gets lost while the remaining part is sent to interact with the sample before reflected towards the detector. The collected light can then be visualized as an interferogram where the intensity signal is a function of the change of the optical pathlength. Finally, a Fourier transform is required to convert the raw data in the interferogram to an absorption spectrum (intensity versus wavenumber).

3.4.4 Diffuse reflectance infrared Fourier transform spectroscopy

In this work, *operando* investigation of surface-bound hydroxyl species on single catalyst components and model catalysts has been carried out by diffuse reflectance infrared Fourier transform spectroscopy (DRIFTS). Experiments in realistic reaction conditions are enabled by a continuous gas flow of reactants through the sample bed along with controlled heating. Reaction kinetics were measured by a mass spectrometer connected to the outlet gas flow. Time-resolved changes of surface-bound species are identified by IR probing using an IR beam directed towards the powder sample. As seen in Figure 3.4, the reflected light is scattered in multiple angles, which is due to both internal

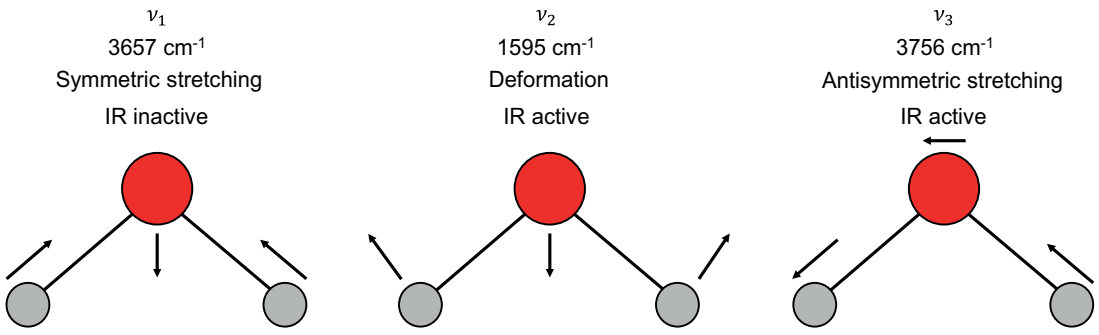

Figure 3.3: Illustration of the vibrational bands of a triatomic non-linear molecule.

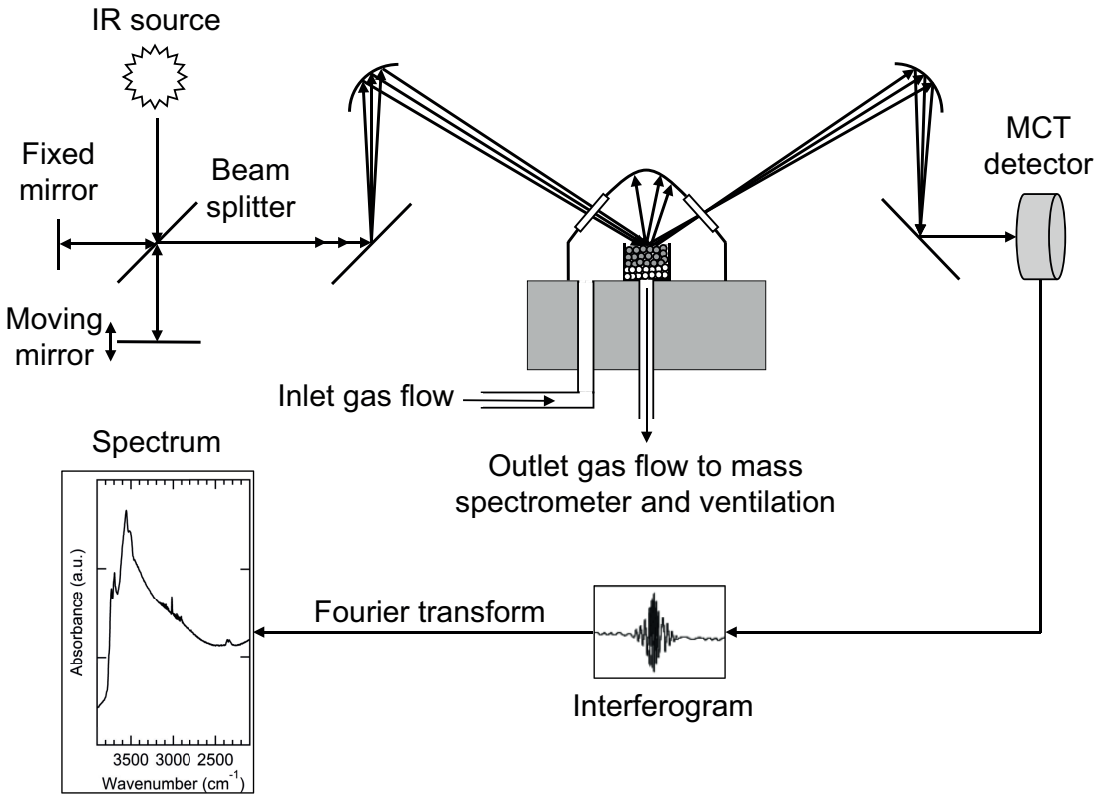

Figure 3.4: Schematic of diffuse reflectance infrared Fourier transform spectroscopy setup

diffusion reflections in the sample and the rough surface of the powder [64]. Elipsodial mirrors are used to focus the incoming light onto the sample as well as collect as much reflected radiation as possible and direct it towards the liquid nitrogen cooled mercury-cadmium-telluride (MCT) detector.

CHAPTER 4
RESULTS AND DISCUSSION

This thesis is based on three independent studies presented in Paper I-III. In the first study (Paper I), oxygen step-response experiments using *operando* X-ray absorption spectroscopy were performed to correlate the state of Pd to CH_4 conversion. The second study (Paper II) show a portable water generator (PWG) device for accurate dosage of low water vapor concentrations (0.1-3.0 vol.%) for reliable spectroscopic and kinetic measurements. The design, operational performance and a case study of water inhibited lean methane oxidation over Pd/Al_2O_3 is described. In the third study (Papaer III) the PWG device is along with *operando* diffuse reflectance infrared Fourier transform spectroscopy, mass spectroscopy, and a bottom-up research approach employed to reveal fundamental understanding of water inhibited methane oxidation. Infrared difference spectra are recorded with both high and low time resolution in dry and wet feeds of O_2 and CH_4 to monitor the rapid and long term build-up of surface-bound hydroxyls (OH) on single catalyst component (PdO and Al_2O_3) and model catalysts (Pd/Al_2O_3) calcined at different temperatures.

4.1 Active state of Pd during lean methane oxidation

The dynamics of how Pd state affects the catalytic activity for methane oxidation were investigated by O_2 step response experiments. Figure 4.1 shows an increased palladium oxide formation rate, in terms of fraction Pd^{2+} (determined by linear combination fitting), with O_2 concentration (0.6, 1.2 and 2.5 vol.%) and reaction temperature (320,

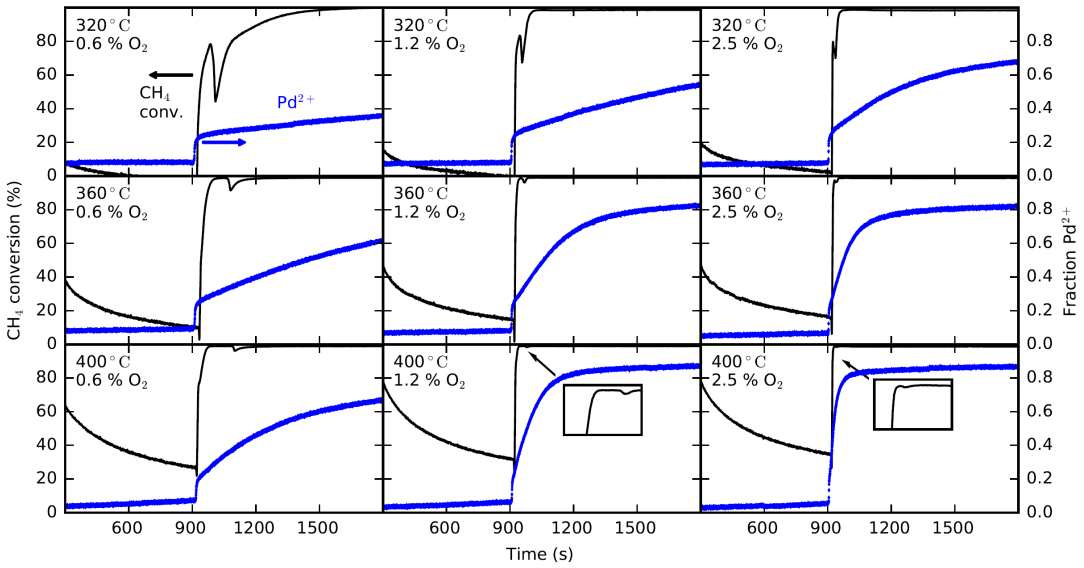

Figure 4.1: The panels show CH_4 conversion and fraction of oxidised Pd during step response experiments over Pd/Al_2O_3 by addition of 0.6, 1.2, or 2.5 vol.% O_2 to a feed of 0.2 vol.% CH_4 at 320, 360 and 400 °C.

360 and 400 °C). The catalytic activity, in terms of CH_4 conversion, is similarly increased when the feed gas composition is switched from a reducing CH_4 flow to net-oxidizing.

A rapidly increased catalytic activity, assigned to CH_4 oxidation over metallic Pd, is followed by a temporary minimum in all experiments when O_2 is added to the feed. The minimum is most pronounced in experiments performed at low temperatures and O_2 concentrations where the rate of Pd oxidation is slow, in accordance to previous results [51, 53]. Small Pd nanoparticles are expected to be bulk oxidized faster than larger ones. Rapid oxidation of these particles explain the instantaneously increased Pd^{2+} fraction in the beginning of the net-oxidising period. Surface oxidation of larger Pd particles will furthermore contribute to the increased Pd^{2+} fraction and previous studies have revealed that a chemisorbed O_2 layer is formed [24, 51]. An oxygen saturated Pd surface is considered to have a low catalytic activity for CH_4 oxidation [65–68], and consequently explains the temporary minimum observed when the fraction of Pd^{2+} is close to 0.3. The larger drop in CH_4 conversion seen in the experiments with slow Pd oxidation, is due to the longer time is required to form an active bulk palladium oxide phase. The results emphasise the importance of operating the catalyst in O_2 excess where the palladium phase is in a bulk oxidised state.

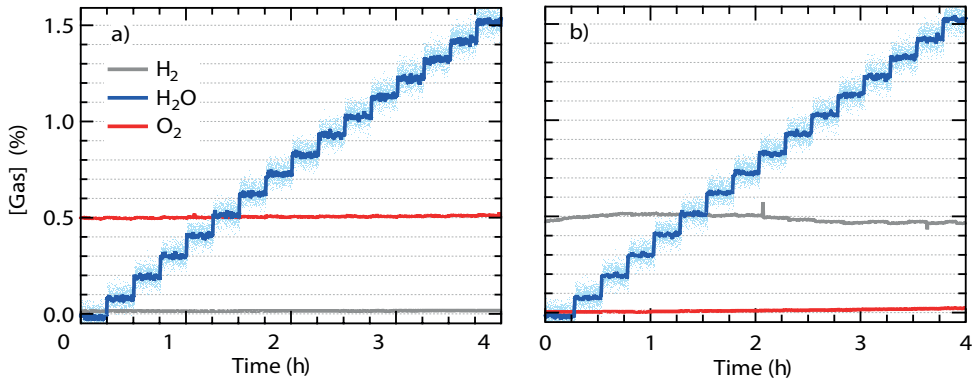

Figure 4.2: Generation of 0-1.5 vol% water vapor in (a) 0.5 vol.% O_2 excess and (b) 0.5 vol.% H_2 excess with argon balance and a total flow of 1500 ml/min. The water signal was smoothed out by averaging 20 experimental values per data point.

4.2 Methane oxidation in dry and wet conditions

4.2.1 Accurate and precise water delivery

To enable reliable spectroscopic studies of the water effect, an accurate and precise supply of water vapor over a range of concentrations is required. Paper II, reports on the design and operational performance of a portable water generator (PWG) device that produces ultra-pure water vapor feeds from catalytic hydrogen oxidation. A Pt/SiO_2 catalyst has both literally and figuratively a central role in the PWG device due to its catalytic properties and position in the middle. Steady operation is ensured by a nozzle heater that surrounds and heat the part of the tube where the catalyst is located to 300 °C. The device is small, light and robust, making lifetime longer and transportation to other research facilities easy. Male connectors are furthermore welded to the inlet and outlet sections of the device to make installation on various systems both on- and off-site fast and durable.

Figure 4.2 shows that the PWG device can provide ultra-pure water vapor of relatively low concentrations (<1.5 vol.%) with high accuracy, which is problematic for commercial systems such as controlled evaporation mixing (CEM). A synthetic gas flow reactor system, usually used for kinetic experiments, was here employed to confirm a successful operational performance in terms of accuracy, stability and response to concentration increments. Depending on desired experimental conditions, it is possible to produce water in either oxygen or hydrogen excess to avoid a slip of the limited reac-

tant. It is furthermore shown in paper II that the PWG device is able to generate water vapor up to at least 3 vol.% at these flow rates (1500 ml/min).

4.2.2 Surface hydroxyls on single catalyst components

Figure 4.3 shows difference IR absorption spectra recorded during an experimental procedure starting (and ending) in a feed of 2% O_2 in argon (bottom/top red), with subsequent addition of CH_4 for 20 min (black) and water for 40 min (blue). The spectra in panel (a) solely show absorption signature bands attributed to gas phase molecules (CH_4, CO_2 and H_2O), i.e. no surface-bound species are observed. A 70% drop in CH_4 turnover frequency (TOF) from 0.0021 to 0.0006 s^{-1} is however seen when going from dry to wet conditions, indicating a strong inhibiting effect at 320 °C. In an attempt to isolate possible stretching modes of hydroxyl groups on PdO, which probably overlaps with water vapor absorption bands, a software (OPUS 7.5) compensation tool for atmospheric water, was used without success. It is likely that the specific surface area of 13 m^2/g for the PdO sample is too low to allow clear detection of hydroxyls even in the case of high coverage and/or the reflectivity of the nearly black powder sample is obscured. Thus, the lack of evidence should not be considered as a proof of non-existence.

In panel b, a flat spectrum is acquired during dry CH_4 oxidation (black spectrum) over γ-Al_2O_3, except for the gas phase methane band at 3000 cm^{-1}, confirming no catalytic activity for the bare support. Addition of water vapor (blue spectrum) gives rise to one negative and four positive IR bands. Our assignment of these bands follow density functional theory (DFT) calculations for the three most common surfaces, i.e., the (100), (110) and (111) facets of γ-Al_2O_3 [69, 70]. The negative IR band with its minimum at 3770 cm^{-1} corresponds to suppression of hydroxyl species with terminal bonding to aluminum cations with octahedral coordination on a (100) facet, $\widetilde{\nu}_{ter}^{OH}(Al_{VI})$, that were still present on the surface after pretreatment when the reference spectrum was recorded. Further, shoulders at 3788 and 3757 cm^{-1} in the negative main band are observed and attributed to hydroxyls with terminal bonding to tetrahedral aluminum cations on a (110) facet, $\widetilde{\nu}_{ter}^{OH}(Al_{IV})$, and triple bridge-bonded hydroxyls to octahedral aluminum cations on a (111) plane, $\widetilde{\nu}_{br}^{OH}(Al_{VI})_3$. During increased coverage of hydroxyl groups with terminal configuration, the negative IR absorbance becomes more pronounced and a perturbed vibrational band, $\widetilde{\nu}_{H-bond}^{OH}(Al_n)$, evolves at 3501 cm^{-1}. A third type of terminal hydroxyl band, $\widetilde{\nu}_{ter}^{OH}(Al_V)$, is seen as a positive peak at 3734 cm^{-1}.

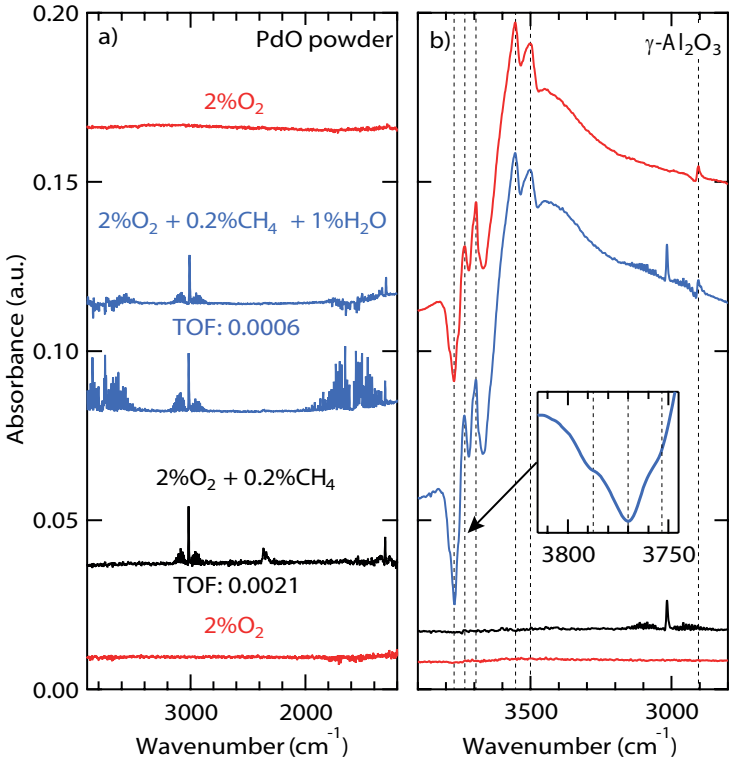

Figure 4.3: IR absorption spectra recorded at 320 °C in 2 % O_2 (bottom red), 20 min in 2.0 vol.% O_2 + 0.2 vol.% CH_4 (black), 40 min in 2.0 vol.% O_2 + 0.2 vol.% CH_4 + 1 vol.% H_2O (blue) and 20 min in 2.0 vol.% O_2 (top red) over unsupported PdO (panel a) and γ-Al_2O_3 (panel b).

This positive peak, however, could also evolve from a bridge-bonded hydroxyl to pentacoordinated aluminum cations, $\tilde{\nu}_{br}^{OH}(Al_V)_2$, having a similar vibration frequency. Two additional bridge-bonded hydroxyls are seen in the blue and red difference spectra at 3694 and 3555 cm^{-1}, denoted $\tilde{\nu}_{br}^{OH}(Al_{VI})_2$ and $\tilde{\nu}_{br}^{OH}(Al_{VI})_3$, respectively.

The top red spectrum recorded in the end of the experiment after 20 minutes of oxygen treatment reveals that the accumulated hydroxyls on the surface are rather stable and require higher temperatures to be decomposed. Interestingly, an unexpected sharp IR band appears at 2905 cm^{-1} when water vapor is introduced to the feed. This band typically evolves from C-H stretching and has been assigned to formate-like species [71, 72]. The band remains even after 20 minutes of oxygen treatment, which signifies a considerable stability of the formate species. The presence of this band suggests that the CH_4 adsorption (interaction) is facilitated over a hydroxylated γ-Al_2O_3 surface, although not catalytically active.

4.2.3 Surface hydroxyls on alumina supported Pd model catalysts

Impact of calcination and reaction temperature

Before discussing the infrared and kinetic results we comment on the physicochemical impact of calcination temperature on the model catalysts. No significant decrease in SSA could be determined for the the Pd/Al_2O_3 model catalysts calcined at 500 and 900 °C, from here denoted PdAl F500 and PdAl F900 respectively. CO chemisorption reveals that high calcination temperature have a negative effect on the palladium surface area that is reduced by more than 50% for PdAl F900 compared to PdAl F500. The increased Pd particle size for PdAl F900 is confirmed by XRD measurements.

Using the same experimental procedure as for the single components, difference spectra recorded at 320 and 440 °C along with CH_4 TOF are shown for PdAl F500 and PdAl F900 in panel a-d of Figure 4.4. Superior catalytic activity is seen in dry conditions for the model catalysts compared to unsupported PdO. When exposed to water, however, the CH_4 TOF drop more for model catalysts, indicating higher susceptibility. PdAl F500 deactivates by about 90% at 320 °C (panel a) and 30% at 440 °C (panel b), as compared to the PdO sample that deactivates by about 70% and 15% at respective temperature. Water inhibition is even stronger over PdAl F900, signifying a severe impact on the palladium-alumina system.

Comparing the difference spectra for PdAl F500 and PdAl F900 with γ-Al_2O_3, some differences are revealed. An extensive build-up of hydroxyl species on alumina is seen already in dry CH_4 oxidation as a consequence of the progressing CH_4 oxidation reaction on the active phase. Addition of 1 vol.% H_2O to the feed results in a substantially increased IR absorption, reaching about the same level for the two catalysts at 320 °C. This reflects that the alumina site density is not severely effected by the calcination process. The lower hydroxyl coverage observed for the two catalysts at 440 °C depends on an increased water desorption rate. This is confirmed by the top red spectra, showing a significantly decreased IR absorption 20 minutes after CH_4 and H_2O was removed from the feed.

Hydroxyl groups formed during dry CH_4 oxidation are clearly not sufficient to saturate the alumina surface and the build-up of hydroxyls from the reaction is likely restricted to the close proximity of the PdO particles. This means that the alumina surface is locally saturated and further hydroxylation of the extended catalyst surface

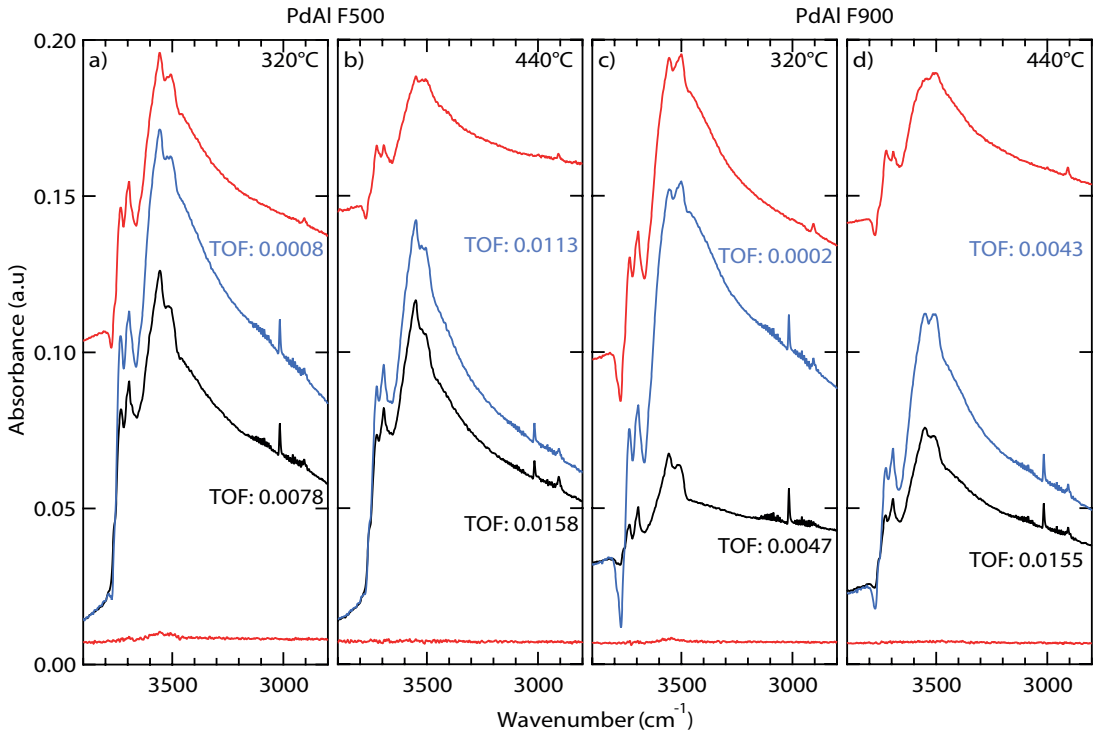

Figure 4.4: IR absorption spectra recorded in 2 % O_2 (bottom red), 20 min in 2.0 vol.% O_2 + 0.2 vol.% CH_4 (black), 40 min in 2.0 vol.% O_2 + 0.2 vol.% CH_4 + 1.0 vol.% H_2O (blue) and 20 min in 2.0 vol.% O_2 (top red) over Pd/γ-Al_2O_3 calcined at 500 °C at a reaction temperature of 320 °C (panel a) and 440 °C (panel b) and Pd/γ-Al_2O_3 calcined at 900 °C at a reaction temperature of 320 °C (panel c) and 440 °C (panel d).

is not possible because of the rather high stability of the hydroxyl species [73]. The larger hydroxyl build-up seen for PdAl F500 strengthened this reasoning since more water is being formed due to higher CH_4 conversion. The lower Pd dispersion and thus less palladium-alumina interface sites could furthermore explain the limited hydroxyl absorbance on PdAl F900.

With a negative terminal IR band, $\tilde{\nu}^{OH}_{ter}(Al_{VI})$, at 3770 cm^{-1} and a pronounced perturbed band, $\tilde{\nu}^{OH}_{H-bond}(Al_n)$, at 3501 cm^{-1}, the spectra recorded over PdAl F900 in wet conditions are more similar to γ-Al_2O_3 compared to PdAl F500. A likely explanation for this is that more concerned Lewis acid sites are blocked by well dispersed Pd as a result of the impregnation and mild calcination for PdAl F500 [74]. Thus, it seems like Pd preferentially occupies aluminum cation sites in vicinity of the terminal bands during preparation and that high temperature treatment leads to sintering of these.

Surface hydroxyl formation routes

A modified experimental procedure was designed to investigate hydroxyl formation routes on PdAl F500. Briefly, the instantaneous build-up of surface hydroxyl groups through dissociation of added water vapor was separated from that of CH_4 oxidation reaction by the use of reference spectra from different conditions, see Figure 4.5. As expected, the largest build-up is observed when 1.0 vol.% H_2O is added to the O_2 treated catalyst surface at 320 °C (panel a). The rate of the instantaneous build-up of $\widetilde{\nu}_{ter}^{OH}(Al_{VI})$, $\widetilde{\nu}_{ter}^{OH}(Al_V)$, $\widetilde{\nu}_{br}^{OH}(Al_{VI})_2$, $\widetilde{\nu}_{br}^{OH}(Al_{VI})_3$ and $\widetilde{\nu}_{H-bond}^{OH}(Al_n)$ species, declines rapidly and the IR bands reach stable absorbances after about 10 min. Thereafter, 0.2 vol.% CH_4 was introduced. Despite the low amount of water formed by the reaction at this temperature a considerable build-up of OH species is seen. Also here, the initial rapid increase in IR absorbance ceases after 10 minutes but compared to the previous distinct spectra, the IR band are not as pronounced.

Performing the experiment at 440 °C leads to significantly decreased absorbance of the IR bands evolved from H_2O dissociation. This is reasonable since the desorption rate is higher and shifts the adsorption-desorption equilibrium towards the gas phase. An opposite trend is however seen for the hydroxyl build-up generated by CH_4 oxidation. Here, the IR absorbance is about twice that observed at 320 °C. Taking into account that the catalytic activity is significantly higher 440 °C, an increased hydroxyl coverage is expected.

This experiment shows that CH_4 oxidation forms surface hydroxyls that are not formed upon water vapor exposure. The same types of hydroxyls seem to form by the two routes and it is not straightforward to conclude whether or not the hydroxyls created by the two routes have a different origin. Reaction mediated hydroxyls are likely formed close to the PdO particles and dissociated hydrogen is necessary.

Deactivation caused by long-term vapor exposure

In addition to the instantaneous deactivation of water, a final study involves the long-term deactivating effect. The panels displayed in Figure 4.6 correlate an increased hydroxyl coverage to declined catalytic activity over PdAl F500 during 24 h dry and wet CH_4 oxidation at 400 °C. A continuous build-up of some hydroxyl bands are observed along with a decreased catalytic activity. The catalyst deactivation is much faster in wet

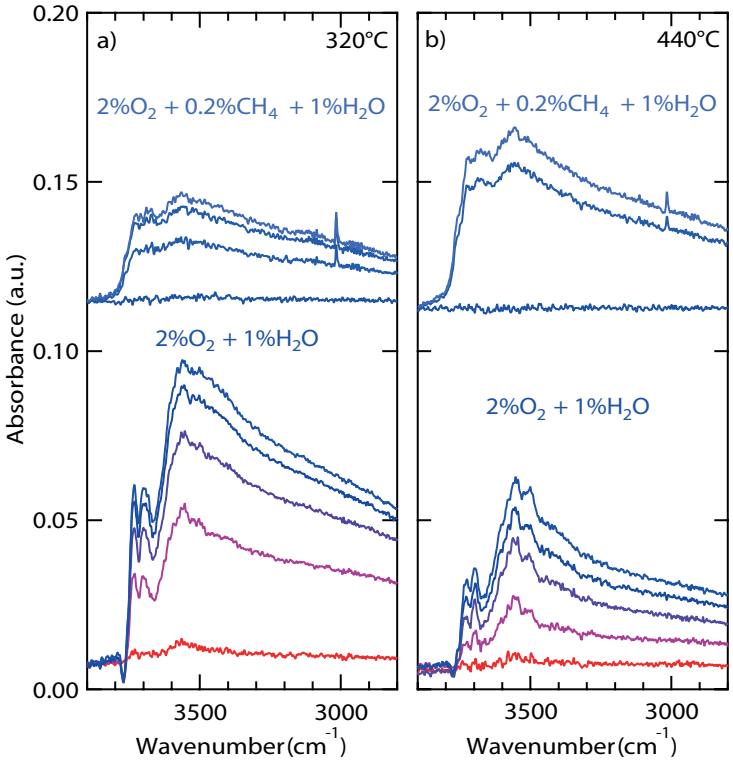

Figure 4.5: Bottom red spectra recorded in 2.0 vol.% O_2 before addition of 1.0 vol.% H_2O kept until steady state where new reference spectra were recorded before 0.2 vol.% CH_4 addition at 320 °C (left) and 440 °C (right).

conditions where the TOF reaches a zero level after five hours. In dry conditions, the experimental time was not sufficiently long to reach steady state. This indicates that the continuous hydroxyl build-up has a negative effect on the reaction kinetics.

An increased IR absorption of the perturbed $\widetilde{\nu}^{OH}_{H-bond}(\mathrm{Al}_n)$ band is observed in both dry and wet conditions. This can be correlated to the negative IR peak area for $\widetilde{\nu}^{OH}_{ter}(\mathrm{Al}_{VI})$ indicating a higher coverage of terminal hydroxyls. The increased hydroxyl coverage over time is also confirmed for the $\widetilde{\nu}^{OH}_{ter}(\mathrm{Al}_V)$ and $\widetilde{\nu}^{OH}_{br}(\mathrm{Al}_{VI})$ bands. Contrary to the already mentioned bands, $\widetilde{\nu}^{OH}_{br}(\mathrm{Al}_{VI})_3$ decreases. Looking at the individual absorbance spectra (not included), it is obvious that the integrated peak area for $\widetilde{\nu}^{OH}_{br}(\mathrm{Al}_{VI})_3$ decreases because it interferes with the evolved $\widetilde{\nu}^{OH}_{H-bond}(\mathrm{Al}_n)$ band, and not because of a lower coverage. The long-term inhibiting effect is hence primarily correlated to an increased coverage of terminal and double bridge-bonded hydroxyl groups. A possible explanation to the long-term inhibiting effect (not proven) could be that water facilitates sintering of small and active PdO cluster that to large extent contribute to the overall CH_4 oxidation. This hypothesis is strengthened by the inability to thermally/-

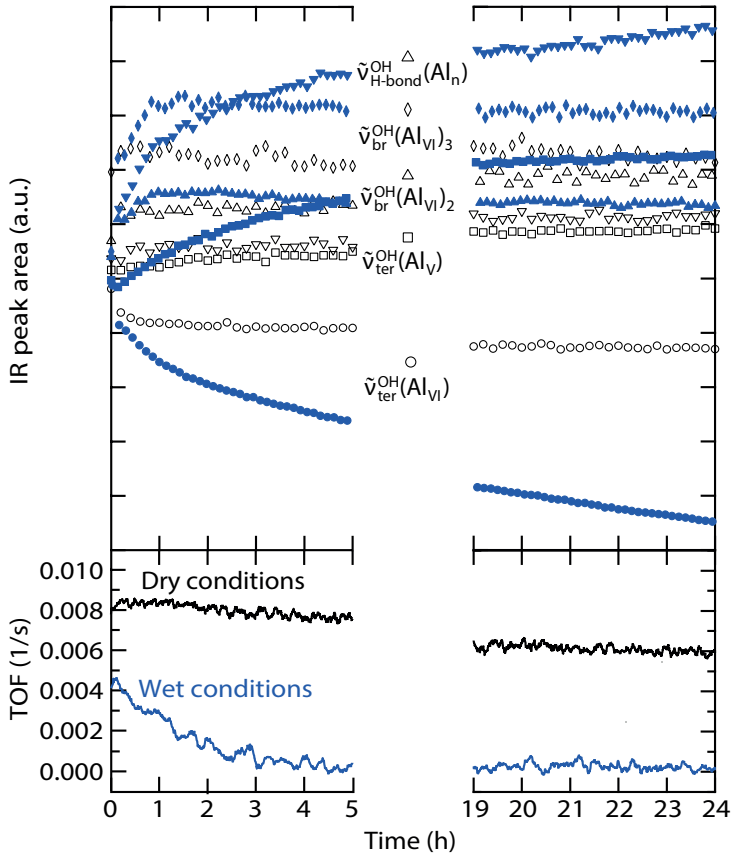

Figure 4.6: 24 h exposure of PdAl F500 to dry (2.0 vol.% O_2 + 0.1 vol.% CH_4) and wet (2.0 vol.% O_2 + 0.1 vol.% CH_4 + 1.0 vol.% H_2O) methane oxidation at 400 °C. Hydroxyl build-up is monitored in the top panel for the $\tilde{\nu}^{OH}_{ter}(Al_n)$ (○), $\tilde{\nu}^{OH}_{ter}(Al_V)$ (□), $\tilde{\nu}^{OH}_{br}(Al_{VI})_2$ (△), $\tilde{\nu}^{OH}_{br}(Al_{VI})_3$ (◊) and $\tilde{\nu}^{OH}_{H-bond}(Al_n)$ (▽) bands where a hollow black marker indicate dry conditions and filled blue marker wet conditions. Catalytic activity is monitored as CH_4 TOF in the bottom panel.

chemically regenerate the catalyst to regain the initial activity.

CHAPTER 5

CONCLUDING REMARKS

In this work the catalytic oxidation of methane in lean conditions is investigated with a focus on the inhibiting effect of water vapor. As reported in Paper I, the conversion rate of CH_4 is highly dependent on the oxidation state of Pd. The states of Pd were experimentally determined by *operando* X-ray absorption spectroscopy as metallic Pd, Pd surface oxidation and a well developed (bulk) PdO. The experiments were carried out under a constant CH_4 flow with successive O_2 exposures. In the absence of O_2, Pd is reduced to metallic Pd and no conversions of CH_4 is observed. Once oxygen is introduced an initial high conversion of CH_4 on Pd occurs. The reaction oxidizes the Pd surface and we see a marked reduction in conversion of CH_4. As the oxidation continues, the palladium particles transitions to bulk PdO, which results in a CH_4 conversion that is higher than for the reduced Pd.

To study the inhibiting effect reported in wet feeds, a portable water vapor generator device was constructed. The design and operational performance is demonstrated in Paper II. The build-up of hydroxyl species on Pd/Al_2O_3 model catalysts and its single catalysts components were monitored in Paper III by connecting the water generator device to an *operando* DRIFTS system. No surface-bound species were detected on pure PdO, which likely results from the low surface area and/or the poor reflectively of the dark powder. A variety of terminal and bridge-bonded hydroxyls were however distinguished on γ-Al_2O_3 and Pd/γ-Al_2O_3. Pd occupying terminal Lewis acid sites on alumina is proposed to explain the absence of a suppressed terminal band and no evolution of a perturbed band for the Pd/γ-Al_2O_3 model catalysts calcined at 500, 650 and 800 °C. It

is further shown that CH_4 oxidation provides an additional channel for formation of surface hydroxyls. The magnitude of hydroxyl formation from solely water produced in the reaction is on the same order as for the experiments using the water generator despite the much lower water concentration produced in the reaction compared to the amount of water added from the generator. One may envisage that these hydroxyl species are formed on preferential sites such as the PdO-Al_2O_3 boundary or in the close proximity of the PdO particles. In addition to a rapid initial hydroxylation, in both dry and wet conditions, a continuous slow build-up is observed during prolonged exposure, which can be correlated to decreased kinetics.

Acknowledgements

The research presented in this thesis was carried out at the Division of Applied Chemistry and the Competence Centre for Catalysis (KCK), Chalmers University of Technology, Göteborg, Sweden, during the period September 2015 to February 2018.

This work is financially supported by the Swedish Energy Agency through the FFI program "Fundamental studies on the influence of water on oxidation catalyst for biogas applications" (No. 40274-1) and the Competence Centre for Catalysis, which is hosted by Chalmers University of Technology and financially supported by the Swedish Energy Agency and the member companies AB Volvo, ECAPS AB, Haldor Topsøe A/S, Scania CV AB, Volvo Car Corporation AB and Wärtsilä Finland Oy.

Parts of the work have also been performed at the European Synchrotron Radiation Facility (ESRF). The provision of beamtime is gratefully acknowedged as well as beamline scientists for their assistance.

I would also like to thank:

My supervisors Per-Anders Carlsson, and co-supervisor Magnus Skoglundh for being enthusiastic and supportive. I really appreciate that your doors are always open and that you create time for discussions, guidance and giving constructive feedback.

Agnes Raj, David Thompsett and Gudmund Smedler for showing great interest in my research, fruitful telecom and face-to-face meetings and creative ideas.

Lennart Norberg, Lasse Urholm and Ulf Stenman for all support in the reactor lab.

Hanna Härelind, Frida Andersson, Lotta Pettersson and Ann Jokobsson for administrative help and all the well-organized events.

My office companion Colin Murphy for nice conversations, grand laughs and a helping hand independently of situation.

Current and and previous colleagues at KCK and TYK for the pleasant working environment and the fun we have both on and off site. Special thanks go to: Alvaro, Andreas, Anna, Carl-Robert, David, Emma, Felix, Giulio, Gustav, Johan, Johanna, Leo, Maria, Mats, Maxime, Mikkel, Milene, Natalia, Saba, Sam, Simone and Ting.

My wonderful girlfriend Josefin! Thanks for always believing in me and making my life divine.

Last but not the least, my mom and my dad for your support and encouragement over the years, you´re the best!

Peter Velin, Göteborg, February 2018

BIBLIOGRAPHY

[1] F. Birol, *International Energy Agency*, 2017, **1**, 1–162.

[2] S. Faramawy, T. Zaki, and A. A. Sakr, *Journal of Natural Gas Science and Engineering*, 2016, **34**, 34–54.

[3] M. Imran, T. Yasmin, and A. Shakoor, *Renewable and Sustainable Energy Reviews*, 2015, **51**, 785–797.

[4] T. Korakianitis, A. M. Namasivayam, and R. J. Crookes, *Progress in Energy and Combustion Science*, 2011, **37**(1), 89–112.

[5] F.-Y. Liang, M. Ryvak, S. Sayeed, and N. Zhao, *Chemistry Central Journal*, 2012, **6**, 1–24.

[6] O. Edenhofer, R. Pichs-Madruga, Y. Sokona, E. Farahani, S. Kadner, K. Seyboth, A. Adler, I. Baum, S. Brunner, P. Eickemeier, B. Kriemann, J. Savolainen, S. Schlömer, C. von Stechow, T. Zwickel, and J. Minx Climate Change 2014: Mitigation of Climate Change Technical report, CAMBRIDGE UNIVERSITY PRESS, 2014.

[7] R. Schlögl, *Angewandte Chemie - International Edition*, 2015, **54**(11), 3465–3520.

[8] A. J. Medford, A. Vojvodic, J. S. Hummelshøj, J. Voss, F. Abild-Pedersen, F. Studt, T. Bligaard, A. Nilsson, and J. K. Nørskov, *Journal of Catalysis*, 2015, **328**(August 2015), 36–42.

[9] R. Burch, D. J. Crittle, and M. J. Hayes, *Catalysis Today*, 1999, **47**, 229–234.

[10] A. A. Latimer, A. R. Kulkarni, H. Aljama, J. H. Montoya, J. S. Yoo, C. Tsai, F. Abild-Pedersen, F. Studt, and J. K. Nørskov, *Nature Materials*, 2016, **1**(October), 1–6.

[11] J. Lampert, M. Kazi, and R. Farrauto, *Applied Catalysis B: Environmental*, 1997, **14**, 211–223.

[12] J. C. van Giezen, F. R. van den Berg, J. L. Kleinen, A. J. van Dillen, and J. W. Geus, *Catalysis Today*, 1999, **47**(1-4), 287–293.

[13] P. Gélin, L. Urfels, M. Primet, and E. Tena, *Catalysis Today*, 2003, **83**(1-4), 45–57.

[14] R. Gholami, M. Alyani, and K. Smith, *Catalysts*, 2015, **5**, 561–594.

[15] G. Koltsakis, *Progress in Energy and Combustion Science*, 1997, **23**(1), 1–39.

[16] C. F. Cullis and D. E. Keene, *Transactions of the Faraday Society*, 1971, **67**, 864–876.

[17] Y.-F. Y. Yao, *Industrial & Engineering Chemistry Product Research and Development*, 1980, **19**, 293–298.

[18] R. F. Hicks, H. Qi, M. L. Young, and R. G. Lee, *Journal of Catalysis*, 1990, **294**, 280–294.

[19] J. Kašpar, P. Fornasiero, and N. Hickey, *Catalysis Today*, 2003, **77**, 419–449.

[20] H. Yamamoto and H. Uchida, *Catalysis Today*, 1998, **45**, 147–151.

[21] K. Narui, H. Yata, K. Furuta, A. Nishida, Y. Kohtoku, and T. Matsuzaki, *Applied Catalysis A: General*, 1999, **179**(1-2), 165–173.

[22] G. Lapisardi, L. Urfels, P. Gélin, M. Primet, A. Kaddouri, E. Garbowski, S. Toppi, and E. Tena, *Catalysis Today*, 2006, **117**(4), 564–568.

[23] R. Abbasi, L. Wu, S. E. Wanke, and R. E. Hayes, *Chemical Engineering Research and Design*, 2012, **90**, 1930–1942.

[24] N. M. Martin, J. Nilsson, M. Skoglundh, E. C. Adams, X. Wang, G. Smedler, A. Raj, D. Thompsett, G. Agostini, S. Carlson, K. Norén, and P.-A. Carlsson, *Catalysis, Structure & Reactivity*, 2017, **3**(1-2), 24–32.

[25] M. Cargnello, J. J. D. Jaen, J. C. H. Garrido, K. Bakhmutsky, T. Montini, J. J. C. Gamez, R. J. Gorte, and P. Fornasiero, *Science*, 2012, **337**(6095), 713–717.

[26] S. Ali, M. J. Al-Marri, A. G. Abdul Monem, Y. I. Arafat, and M. M. Khader, *Proceedings of the 4th International Gas Processing Symposium*, 2015, pp. 89–97.

[27] J. Chen, H. Arandiyan, X. Gao, and J. Li, *Catalysis Surveys from Asia*, 2015, **19**(3), 140–171.

[28] M. Monai, T. Montini, C. Chen, E. Fonda, R. J. Gorte, and P. Fornasiero, *ChemCatChem*, 2015, **7**(14), 2038–2046.

[29] F. F. Tao, J.-J. Shan, L. Nguyen, Z. Wang, S. Zhang, L. Zhang, Z. Wu, W. Huang, S. Zeng, and P. Hu, *Nature communications*, 2015, **6**, 7798.

[30] Y. Wang, H. Arandiyan, J. Scott, M. Akia, H. Dai, J. Deng, K. F. Aguey-Zinsou, and R. Amal, *ACS Catalysis*, 2016, **6**(10), 6935–6947.

[31] X. Zhao, Y. Liu, J. Deng, P. Xu, J. Yang, K. Zhang, Z. Han, and H. Dai, *Molecular Catalysis*, 2017, **442**, 191–201.

[32] C. H. Bartholomew, *Applied Catalysis A: General*, 2001, **212**(1-2), 17–60.

[33] D. Ciuparu, N. Katsikis, and L. Pfefferle, *Applied Catalysis A: General*, 2001, **216**(1-2), 209–215.

[34] R. Kikuchi, S. Maeda, K. Sasaki, S. Wennerström, and K. Eguchi, *Applied Catalysis A: General*, 2002, **232**(1-2), 23–28.

[35] K. Persson, L. D. Pfefferle, W. Schwartz, A. Ersson, and S. G. Järås, *Applied Catalysis B: Environmental*, 2007, **74**(3-4), 242–250.

[36] C. F. Cullis, T. G. Nevell, and D. L. Trimm, *Journal of the Chemical Society, Faraday Transactions 1*, 1972, **68**, 1406.

[37] D. Roth, P. Gélin, M. Primet, and E. Tena, *Applied Catalysis A: General*, 2000, **203**(1), 37–45.

[38] R. Burch, F. Urbano, and P. Loader, *Applied Catalysis A: General*, 1995, **123**(1), 173–184.

[39] G. A. O. Diannan, W. Sheng, Z. Chunxi, Y. Zhongshan, and W. Shudong, *Chinese Journal of Catalysis*, 2008, **29**(12), 1221–1225.

[40] D. Ciuparu, E. Perkins, and L. Pfefferle, *Applied Catalysis A: General*, 2004, **263**(2), 145–153.

[41] W. R. Schwartz, D. Ciuparu, and L. D. Pfefferle, *Journal of Physical Chemistry C*, 2012, **116**(15), 8587–8593.

[42] W. R. Schwartz and L. D. Pfefferle, *Journal of Physical Chemistry C*, 2012, **116**(15), 8571–8578.

[43] C. A. Mu, M. Maciejewski, A. Koeppel, R. Tschan, and A. Baiker, *Journal of Physical Chemistry*, 1996, **100**(51), 20006–20014.

[44] J. Au-Yeung, K. Chen, A. T. Bell, and E. Iglesia, *Journal of Catalysis*, 1999, **188**(1), 132–139.

[45] M. Van Den Bossche and H. Grönbeck, *Journal of the American Chemical Society*, 2015, **137**(37), 12035–12044.

[46] Y. Ozawa, Y. Tochihara, A. Watanabe, M. Nagai, and S. Omi, *Applied Catalysis A, General*, 2004, **259**(3), 1–7.

[47] C. L. Pieck, C. R. Vera, E. M. Peirotti, and J. C. Yori, *Applied Catalysis A, General*, 2002, **226**, 281–291.

[48] G. Ketteler, D. F. Ogletree, H. Bluhm, H. Liu, E. L. Hebenstreit, and M. Salmeron, *Journal of the American Chemical Society*, 2005, **127**(51), 18269–18273.

[49] R. J. Farrauto, J. K. Lampert, M. C. Hobson, and E. M. Waterman, *Applied Catalysis B, Environmental*, 1995, **6**(3), 263–270.

[50] E. Lundgren, J. Gustafson, a. Mikkelsen, J. N. Andersen, a. Stierle, H. Dosch, M. Todorova, J. Rogal, K. Reuter, and M. Scheffler, *Physical review letters*, 2004, **92**(4), 046101.

[51] J. Nilsson, P. A. Carlsson, N. M. Martin, E. C. Adams, G. Agostini, H. Grönbeck, and M. Skoglundh, *Journal of Catalysis*, 2017, **356**, 237–245.

[52] N. M. Martin, J. Nilsson, M. Skoglundh, E. C. Adams, X. Wang, P. Velin, G. Smedler, A. Raj, D. Thompsett, H. H. Brongersma, T. Grehl, G. Agostini, O. Mathon, S. Carlson, K. Nore, F. J. Martinez-casado, Z. Matej, O. Balmes, and P.-a. Carlsson, *Journal of Physical Chemistry C*, 2016, **120**, 28009–28020.

[53] J. Nilsson, P.-A. Carlsson, S. Fouladvand, N. M. Martin, J. Gustafson, M. A. Newton, E. Lundgren, H. Grönbeck, and M. Skoglundh, *ACS Catalysis*, 2015, **5**(4), 2481–2489.

[54] P. Munnik, P. E. De Jongh, and K. P. De Jong, *Chemical Reviews*, 2015, **115**(14), 6687–6718.

[55] P. H. Emmett, *Journal of the American Chemical Society*, 1936, **60**(2), 309–319.

[56] P. Canton, G. Fagherazzi, M. Battagliarin, F. Menegazzo, F. Pinna, and N. Pernicone, *Langmuir*, 2002, **18**, 6530–6535.

[57] C. G. Pope, *Journal of Chemical Education*, 1997, **74**(1), 129–131.

[58] A. J. C. Wilson, *Journal of Applied Crystallography*, 1978, **11**, 102–113.

[59] A. Chakrabarti, M. E. Ford, D. Gregory, R. Hu, C. J. Keturakis, S. Lwin, Y. Tang, Z. Yang, M. Zhu, M. A. Bañares, and I. E. Wachs, *Catalysis Today*, 2017, **283**, 27–53.

[60] A. Urakawa, *Current Opinion in Chemical Engineering*, 2016, **12**, 31–36.

[61] S. Pascarelli, G. Aquilanti, L. Dubrovinsky, G. Guilera, O. Mathon, M. Munoz, M. A. Newton, M. Pasquale, A. Trapananti, E. Synchrotron, R. Facility, and J. Horowitz

In *AIP Conference Proceedings*, Vol. 882, pp. 608–612, 2007.

[62] S. Pascarelli, O. Mathon, T. Mairs, I. Kantor, G. Agostini, and C. Strohm, *Journal of Synchrotron Radiation*, 2016, **23**, 353–368.

[63] H. Günzler and H.-U. Gremlich, *IR Spectroscopy - An Introduction*, WILEY-VCH, 2002.

[64] Z. M. Khoshhesab, *Reflectance IR Spectroscopy*, InTech, 2012.

[65] N. M. Martin, M. Van Den Bossche, A. Hellman, H. Grönbeck, C. Hakanoglu, J. Gustafson, S. Blomberg, N. Johansson, Z. Liu, S. Axnanda, J. F. Weaver, and E. Lundgren, *ACS Catalysis*, 2014, **4**(10), 3330–3334.

[66] Y. H. Chin, C. Buda, M. Neurock, and E. Iglesia, *Journal of the American Chemical Society*, 2013, **135**(41), 15425–15442.

[67] X. Weng, H. Ren, M. Chen, and H. Wan, *ACS Catalysis*, 2014, **4**(8), 2598–2604.

[68] P. A. Carlsson, E. Fridell, and M. Skoglundh, *Catalysis Letters*, 2007, **115**(1-2), 1–7.

[69] M. Digne, P. Sautet, P. Raybaud, P. Euzen, and H. Toulhoat, *Journal of Catalysis*, 2002, **211**(1), 1–5.

[70] M. Digne, P. Sautet, P. Raybaud, P. Euzen, and H. Toulhoat, *Journal of Catalysis*, 2004, **226**(1), 54–68.

[71] G. Busca, J. Lamotte, J. ciaude Lavalley, and V. Lorenzelli, *Journal of the American Chemical Society*, 1987, **109**(17), 5197–5202.

[72] P. J. Jodłowski, R. J. Jędrzejczyk, D. Chlebda, M. Gierada, and J. Łojewska, *Journal of Catalysis*, 2017, **350**, 1–12.

[73] O. Mihai, G. Smedler, U. Nylén, M. Olofsson, and L. Olsson, *Catal. Sci. Technol.*, 2017, **7**(14), 3084–3096.

[74] A. B. M. Saad, V. A. Ivanov, J. C. Lavalley, P. Nortier, and F. Luck, *Applied Catalysis A, General*, 1993, **94**(1), 71–83.